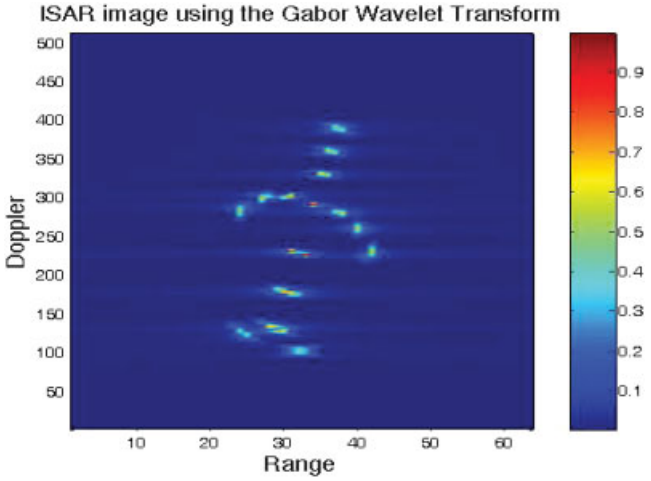

Figure 12 Ideal point scatterers ISAR image using the MEM and GWT, the 200th frame. [Color figure can be viewed in the online issue, which is available at www.interscience.wiley.com]

suggested approach is an excellent candidate for noncooperative target recognition (NCTR). To show the performances of each algorithm, we use backscattered field data of the ideal point scatterers and the simulated MIG-25 to obtain motion compensated ISAR image, and display the resolution of motion compensated ISAR images.

ACKNOWLEDGMENT

This research was supported by the Agency for Defense Development, Korea, through the Radiowave Detection Research Center at the Korea Advanced Institute of Science and Technology.

REFERENCES

1. V.C. Chen and S. Qian, Joint time-frequency transform for radar range-doppler imaging, IEEE Trans Aerospace Electron Syst 34 (1998), 486–499.
2. V.C. Chen, Applications of time-frequency processing to radar imaging, Proc SPIE 2762 (1996), 23–31.
3. L.C. Potter, D.M. Chiang, R. Carriere, and M.J. Gerry, GTD-based parametric model for radar scattering, IEEE Trans Antennas Propagat 43 (1995), 1058–1067.
4. L. Du and G. Su, Adaptive inverse synthetic aperture radar imaging for nonuniformly moving targets, IEEE Geosci Remote Sens Lett 2 (2005), 247–249.
5. G.Y. Wang and Z. Bao, The minimum entropy criterion of range alignment in ISAR motion compensation, Proc Radar Conf (1999), 236–239.
6. Z. Liu and S. Zhang, A novel method of translational motion compensation for hopped-frequency isar imaging, IEEE Int Radar Conf (2000), 255–260.
7. L. Xi, L. Guosui, and J. Ni, Autofocusing of ISAR image based on entropy minimization, IEEE Trans Aerospace Electron Syst 35 (1999), 1240–1252.
8. S. Qian and D. Chen, Joint time-frequency analysis methods and applications, Prentice Hall PTR, San Francisco, CA 1996.
9. T.S. Lee, Image representation using 2D Gabor wavelets, PAMI, IEEE Trans 18 (1996), 959–971.
10. J.S. Son, G. Thomas, and B.C. Flores, Range-doppler radar image and motion compensation, Artech House, Norwood, MA 2001.

COMPACT DUAL BAND WILKINSON POWER DIVIDER

Ashraf S. S. Mohra
Department of Electrical Engineering, College of Engineering, King Saud University, P.O 800, Riyadh 11421, Saudi Arabia;
Corresponding author: amohra@ksu.edu.sa

Received 29 October 2007

ABSTRACT: *This article presents the design of a compact Wilkinson power divider for dual applications. The design is accomplished by transforming the length and impedance of the quarter wave sections of the conventional Wilkinson power divider into dual band* Π*-shaped sections. Simple design equations for basic design geometry are given. The dual band power divider geometry is analyzed using EM simulator and then realized at 1.8 and 4.775 GHz.* © 2008 Wiley Periodicals, Inc. Microwave Opt Technol Lett 50: 1678–1682, 2008; Published online in Wiley InterScience (www.interscience.wiley.com). DOI 10.1002/mop.23465

Key words: *dual band; Wilkinson power divider;* Π*-shaped; microstrip*

1. INTRODUCTION

The Wilkinson power divider is one of the most commonly used components in wireless communication system for power division and/or combination. The Wilkinson power divider was invented in 1960 [1] and has completely matched output ports with sufficiently high isolation between them. The power divider consists of two ($\lambda/4$) branches of transmission line and a termination resistor of 100 Ω, where λ is the wavelength of the transmission line, Figure 1. The power divider used in different microwave circuit such as push-pull amplifiers, balanced mixers, and antenna distribution circuits. Recent years have seen a worldwide effort to develop dual-band power dividers [2–8] due to the trend of multiband applications. A conventional Wilkinson power divider operates only at one design frequency and at its odd harmonics, therefore, it is not suitable for some dual-band operations. A numerically nearly exact solution for a Wilkinson power divider operating at a design frequency and simultaneously at its first even harmonic has been presented at [2]. Later the authors [3] designed a power divider that can operate at any two different frequencies by replace each quarter-wave branch of a conventional Wilkinson power divider with two sections of transmission line with the characteristic impedance of z_1 and z_2 and lengths of l_1 and l_2, respectively, while the output ports are shunted with a parallel connection of a resistor, an inductor, and a capacitor, Figure 2(a). Recently Cheng

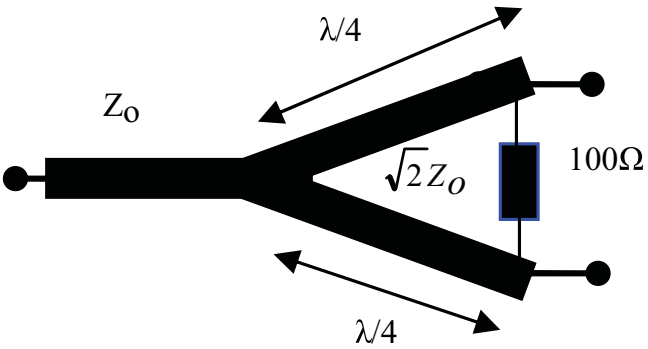

Figure 1 Conventional Wilkinson power divider. [Color figure can be viewed in the online issue, which is available at www.interscience.wiley.com]

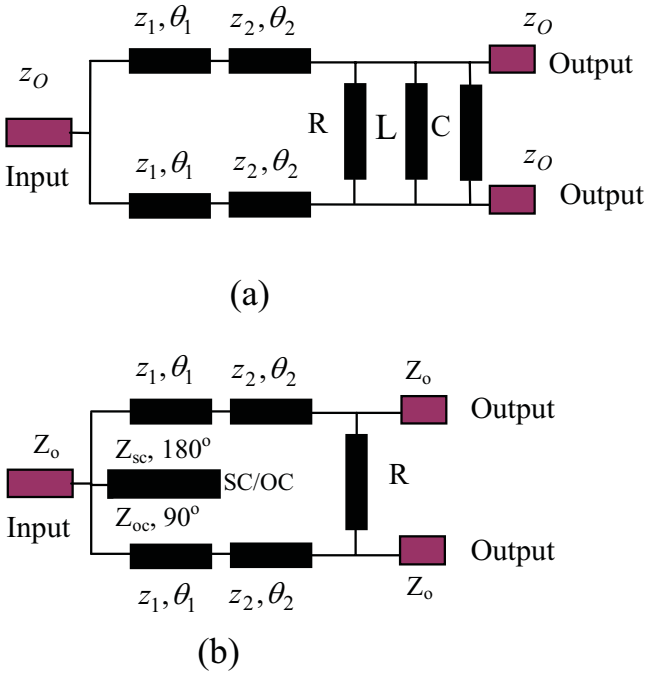

Figure 2 Dual band Wilkinson power divider. (a) Using cascaded sections and lumped parameters [3]. (b) Using cascaded and SC/OC sections and resistor [4]. [Color figure can be viewed in the online issue, which is available at www.interscience.wiley.com]

and Wong [4] replaced the lumped elements L and C with SC/OC shunt stub transmission line in front of the two cascaded sections of the transmission line that used at [3], Figure 2(b). In fact, the size of the dual band Wilkinson power dividers that used at [3, 4] still have a large geometrical dimensions due to the cascaded transmission lines.

In this article, we present a new design of compact dual-band Wilkinson power divider. This power divider consists of replacing each ($\lambda/4$) section of the conventional Wilkinson power divider, Figure 1, with its corresponding Π-section, Figure 3(b). The analytical solution for the transition of the quarter wave transmission line to Π-section that operates at two arbitrary frequencies is demonstrated in Section 2. The analysis and measurements of the dual band Wilkinson power divider will be given in Section 3.

2. ANALYSIS OF DUAL BAND Π-SHAPED TRANSMISSION LINE

Each quarter wavelength ($\lambda/4$) section of the conventional Wilkinson power divider, Figure 1, will be converted to a dual band Π-shaped transmission line model. The Π-shaped transmission line model shown in Figure 3(b) is consisted of two identical shunt open stubs and one series transmission line connecting the two stubs. The equivalence between the ($\lambda/4$) transmission line sections of Figure 3(a) and the Π-section is investigated utilizing the ABCD matrices for both sections.

The ABCD matrix for the original transmission line of Figure 3(a), with ($\lambda/4$) length is given by

$$M_1 = \begin{bmatrix} 0 & jz_1 \\ jy_1 & 0 \end{bmatrix} \tag{1}$$

The ABCD matrix for the Π-shaped transmission line section of Figure 3(b) is

$$M_T = M_3 M_2 M_3 \tag{2}$$

where M_2 and M_3 are defined as:

$$M_2 = \begin{bmatrix} \cos\theta_2 & jz_2\sin\theta_2 \\ jy_2\sin\theta_2 & \cos\theta_2 \end{bmatrix} \tag{3a}$$

$$M_3 = \begin{bmatrix} 1 & 0 \\ jy_3\tan\theta_3 & 1 \end{bmatrix} \tag{3b}$$

Equating the element A of the ABCD matrix from Eqs. (1) and (2), the relation between the elements of the $\prod$ -shape section can be given as follows:

$$\tan\theta_3 = \frac{Z_3}{Z_2}\cot(\theta_2) \tag{4}$$

Equating the element B of the ABCD matrix from Eqs. (1) and (2), the following equation is obtained

$$z_1 = z_2\sin\theta_2 \tag{5}$$

For the purpose of dual band operation, it is necessary to modify Eq. (5) as follows [9]:

$$z_2\sin\theta_{2f_1} = \pm z_1 \tag{6a}$$

$$z_2\sin\theta_{2f_2} = \pm z_1 \tag{6b}$$

where θ_{2f_1} and θ_{2f_2} are the electrical lengths of the series element of the Π-section at the two operating frequencies f_1 and f_2 respectively, where ($f_2 > f_1$). The solution for Eq. (6) is given by:

$$\theta_{2f_2} = n\pi - \theta_{2f_1}, n = 1,2,3\ldots \tag{7}$$

For compact size, choose $n = 1$. The relation between the electrical lengths and the dual band operating frequencies must be as:

$$\frac{\theta_{2f_2}}{\theta_{2f_1}} = \frac{f_2}{f_1} = R \tag{8}$$

Equation (8) can be modified by using Eq. (7) to the following form:

$$\theta_{2f_1} = \frac{n\pi}{R+1} \tag{9}$$

$$\theta_{2f_2} = \frac{Rn\pi}{R+1} \tag{10}$$

Based on Eqs. (4) and (8), the following conditions can be deduced for (θ_3):

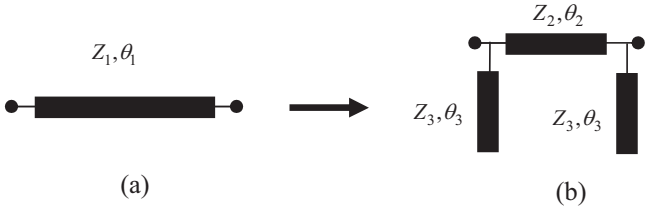

Figure 3 (a) Transmission line section. (b) Π-equivalent section

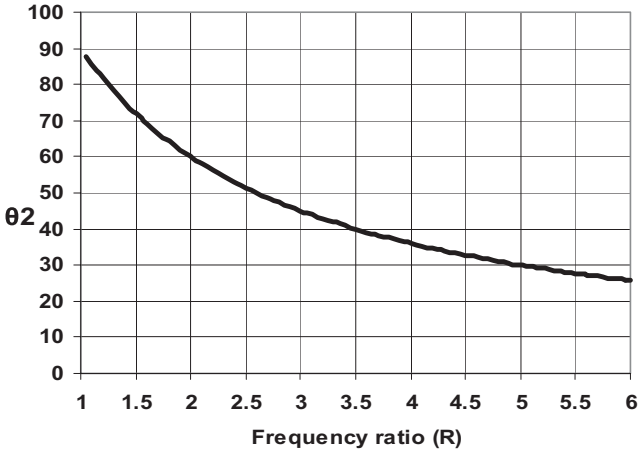

Figure 4 The electrical length against frequency ratio R

$$\theta_{3f_2} = m\pi - \theta_{3f_1}, m = 1,2,3\ldots \tag{11}$$

$$\frac{\theta_{3f_2}}{\theta_{3f_1}} = \frac{f_2}{f_1} = R \tag{12}$$

Equations (11) and (12) can be modified to the following relations:

$$\theta_{3f_1} = \frac{m\pi}{R+1} \tag{13}$$

$$\theta_{3f_2} = \frac{Rm\pi}{R+1} \tag{14}$$

For compact design, $m = 1$ is chosen. From the above equations it is found that, the electrical lengths of a practical Π -shape section must be bounded in these regions ($\pi/4 \leq \theta_2, \theta_3 \leq \pi/2$). The design procedure for the compact dual band Wilkinson power divider that operates at dual band can be presented as follows:

-The value of the required frequency ratio R is found from Eq. (8).
-The electrical length corresponding to series transmission line is found from Eq. (9), with $n = 1$ for compact size.

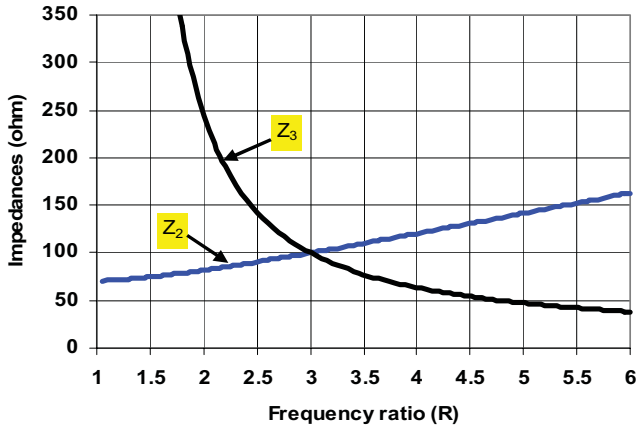

Figure 5 Impedance variations against frequency ratio R. [Color figure can be viewed in the online issue, which is available at www.interscience.wiley.com]

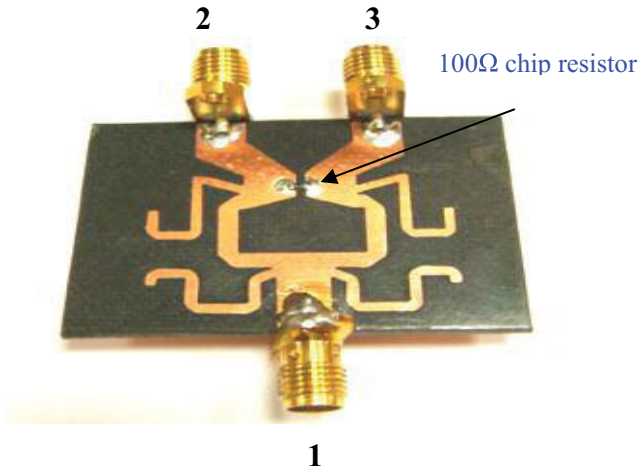

Figure 6 The realized dual band Wilkinson power divider. [Color figure can be viewed in the online issue, which is available at www.interscience.wiley.com]

-The electrical length corresponding to shunt stub is found from Eq. (13), with $m = 1$ for compact size.
-The values of impedances z_2 and z_3 can be calculated as follows:

$$z_2 = \frac{z_1}{\sin(\theta_{2f_1})} \tag{15a}$$

$$z_3 = z_2 \cdot \tan(\theta_{2f_1}) \cdot \tan(\theta_{3f_1}) \tag{15b}$$

Figure 4 illustrates the variations of electrical lengths θ_{2f_1} ($\theta_{3f_1} = \theta_{2f_1}$) against the frequency ratio R, while Figure 5 illustrates the variation of the characteristic impedances z_2 and z_3 against the frequency ratio R. For practical realization of microstrip lines, the characteristic impedance should be bounded in the region ($30\ \Omega \leq Z \leq 150\ \Omega$), so the corresponding practical frequency ratio must be in the range ($1.85 \leq R \leq 5$).

3. SIMULATION AND MEASUREMENTS OF THE DUAL BAND WILKINSON POWER DIVIDER

The dual band Wilkinson power divider was designed for two frequencies which are $f_1 = 1.8$ GHz and $f_2 = 4.775$ GHz. With the design procedure that described in Section 2, while $z_1 = 70.711\ \Omega$,

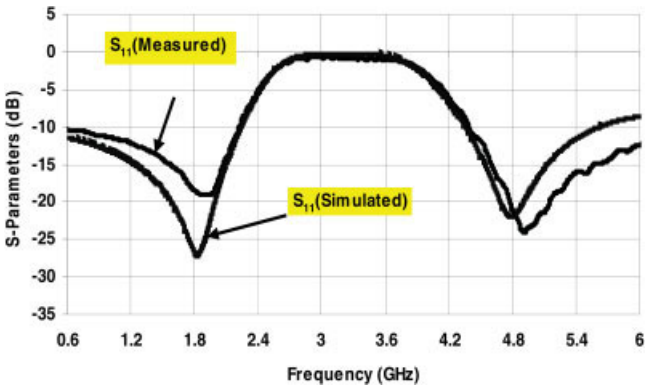

Figure 7 Simulated and measured return loss (S_{11}). [Color figure can be viewed in the online issue, which is available at www.interscience.wiley.com]

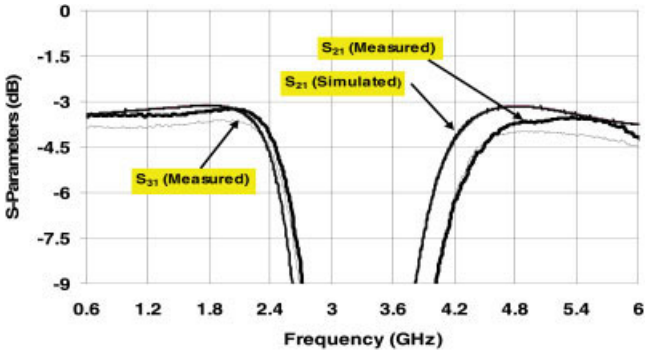

Figure 8 Simulated and measured insertion loss (S_{21}, S_{31}). [Color figure can be viewed in the online issue, which is available at www.interscience.wiley.com]

the design parameters realized on RT/Duriod5880 Teflon substrate $\{\varepsilon_r = 2.2, h = 1.5748 \text{ mm}\}$ will be ($z_2 = 93.3\ \Omega$, $z_3 = 125.91\ \Omega$, $\theta_2 = \theta_3 = 49.28°$). The dual band power divider was simulated using IE3D software package [10]. The circuit has been realized and a chip resistor (100 Ω) was soldered between output ports, Figure 6. The scattering parameters were measured and compared with the simulated results in Figures 7–10. It is clear that, the measured input return loss (S_{11}) are less than (−18 dB) *at* f_1 (1.8 GHz) and less than (−20 dB) *at* f_2 (4.775 GHz). When we consider S_{11} less than (−15 dB), *then bandwidth will be* 27% *at the first frequency* f_1, and will be greater 19% at the second frequency f_2. The simulated insertion coefficients (S_{21}) and (S_{31}) are identical, so only simulated (S_{21}) is shown in Figure 8. The insertion coefficient (S_{21}) is nearly the same for simulation and measurements with 0.2-dB deviation at f_1 and a 0.55-dB deviation at f_2. The measured insertion coefficient S_{31} deviates by 0.6 dB at f_1 and 0.65 dB at f_2. The output return loss (S_{22}) is less than −18 dB for f_1 and less than −25 dB for f_2. The output port isolation S_{32} is less than −18 dB for first frequency and less than −22 dB for second frequency. The phase response is shown in Figure 11, in which it is clear that the phase deviation is around 0.5° at first frequency and less than 0.8° at second frequency. The overall geometrical dimensions of the realized dual band Wilkinson power divider is 870.16 mm^2 which represent around 0.65% of the corresponding dimension needed for the dual frequency Wilkinson

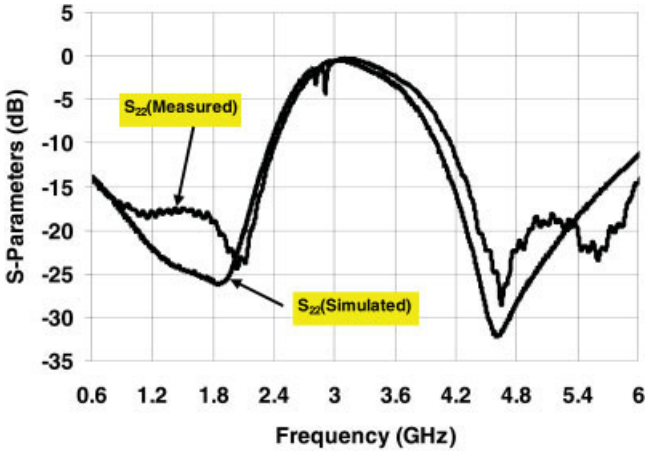

Figure 9 Simulated and measured output return loss (S_{22}). [Color figure can be viewed in the online issue, which is available at www.interscience.wiley.com]

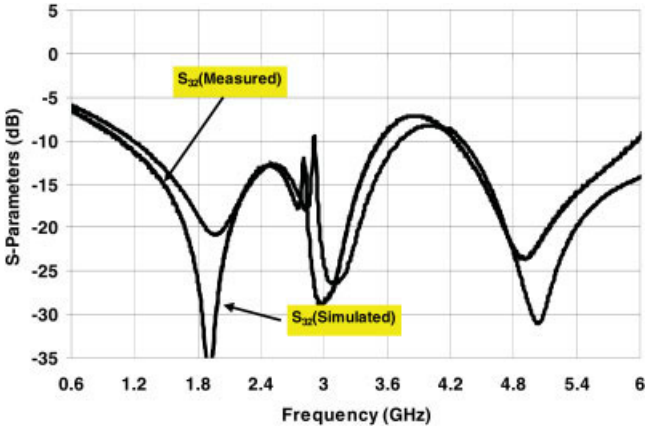

Figure 10 Simulated and measured output port isolation (S_{32}). [Color figure can be viewed in the online issue, which is available at www.interscience.wiley.com]

power divider presented at [2, 3] which was designed on the same substrate materials. So, the design of dual band Wilkinson power divider using the Π-section transformation makes the overall geometrical dimensions is small.

4. CONCLUSION

This article presents analysis and design of a compact dual band Wilkinson power divider. The basic design uses dual band Π -section transformation of the quarter wavelength sections of the power divider with no short circuit stubs or via holes. Practical and simple design equations are presented. A compact dual band Wilkinson power divider is designed and examined using a full wave EM software simulator and then realized on RT/Duroid 5880 substrate $\{\varepsilon_r = 2.2, h = 1.5748 \text{ mm}\}$. The measurements of the realized dual-band Wilkinson power divider are in good agreement with the simulated results. For the dual band Wilkinson power divider, the coupling is (−3 dB) with a little variation less than 0.65 dB for both of the operating bands and the phase difference between output ports not exceed 0.8°. The realized dual band Wilkinson power divider is compact because it represents around 0.65% of the dual band Wilkinson power divider using cascaded two transmission line sections and lumped parameters *R*, *L*, and *C*.

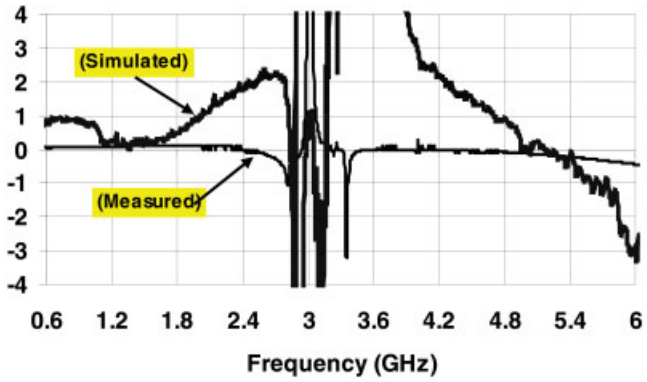

Figure 11 Simulated and measured phase response. [Color figure can be viewed in the online issue, which is available at www.interscience.wiley.com]

REFERENCES

1. E. Wilkinson, An N-way hybrid power divider, IRE Trans Microwave Theory Tech MTT-8 (1960), 116–118.
2. L. Wu, H. Yilmaz, T. Bitzer, A. Pascht, and M. Berroth, A dual-frequency Wilkinson power divider: For a frequency and its first harmonic, IEEE Microwave Wireless Compon Lett 5 (2005), 107–109.
3. L. Wu, Z. Sun, H. Yilmaz, and M. Berroth, A dual band frequency Wilkinson power divider, IEEE Trans Microwave Theory Tech 54 (2006), 278–284.
4. K. Cheng and F. Wong, A new Wilkinson power divider design for dual band application, IEEE Microwave Wireless Compon Lett 17 (2007), 664–666.
5. J.H. Sung, G.Y. Kim, S.H. Son, H.J. Lee, Y.J. Song, Y.W. Jeong, H.S. Park, and D. Ahn, Design method of a dual band balun and divider, IEEE MTT-S Int Microwave Symp Dig 2 (2002), 1177–1180.
6. K.L. Wan, Y.L. Chow, and K.M. Luk, Simple design of dual-frequency unequal power-divider, Electron Lett 37 (2001), 1171–1173.
7. S. Avrillon, I. Pele, A. Chousseaud, and S. Toutain, Dual-band power divider based on semiloop stepped-impedance resonators, IEEE Trans Microwave Theory Tech 51 (2003), 1269–1273.
8. I. Lin, M. Vincentis, C. Caloz, and T. Itoh, Arbitrary dual-band components using composite right/left-hand transmission lines, IEEE Trans Microwave Theory Tech 52 (2004), 1142–1149.
9. K. Keung, M. Cheng, and F.-L. Wong, A novel approach to the design and implementation of dual-band compact planar 90° branch-line coupler, IEEE Trans Microwave Theory Tech 52 (2004), 2458–2463.
10. Zeland software, Version. 9.35, Zeland Company, 2002.

DIVIDE-BY-3 INJECTION-LOCKED FREQUENCY DIVIDER IMPLEMENTED WITH ACTIVE INDUCTOR

Sheng-Lyang Jang, Chia-Wei Tai, and Chien-Feng Lee
Department of Electronic Engineering, National Taiwan University of Science and Technology, 43 Keelung Road, Section 4, Taipei, Taiwan 106, Republic of China; Corresponding author: D9202209@mail.ntust.edu.tw

Received 4 November 2007

ABSTRACT: *This article presents a wide locking-range divide-by-3 injection-locked frequency divider (ILFD) employing tunable active inductors (TAIs), which are used to extend the locking range and to reduce die area. The CMOS ILFD is based on a voltage-controlled oscillator (VCO) with cross-coupled switching pairs and TAI-C tanks, and was fabricated in the 0.18-μm 1P6M CMOS technology. The divide-by-3 function is performed by injecting differential signal to the gates of two injection MOSFETs with the drains connected to the VCO outputs and with grounded sources. Measurement results show that at the supply voltage of 1.8 V, the divider free-running frequency is tunable from 1.20 to 1.284 GHz, and at the incident power of 4 dBm the locking range is about 1.9 GHz (45.2%), from the incident frequency 3.3 to 5.2 GHz. The core power consumption is 12.96 mW. The die area is 0.45 × 0.513 mm².* © 2008 Wiley Periodicals, Inc. Microwave Opt Technol Lett 50: 1682–1685, 2008; Published online in Wiley InterScience (www.interscience.wiley.com). DOI 10.1002/mop.23458

Key words: *CMOS; divide-by-3 injection-locked frequency divider; locking range; tunable active inductor*

1. INTRODUCTION

Frequency divider (FD) has received a greater attention in the past for application in frequency synthesizers and signal generators. FDs can take a periodic input signal and generate a periodic output signal at a frequency that is a fraction of the input signal. The LC resonator-based injection-locked frequency divider (ILFD) is often used because the operating frequency can be very high and the divider consumes low power. The divide-by-2 ILFD [1, 2] has been well studied because of binary function leading to easy design and application; however, the divide-by-3 ILFD [3-5] has received much less attention.

At low GHz range, using passive inductor results in large chip area and increases the cost of production. To lower the product cost, the passive inductor can be replaced by active inductor. Recently, active inductors have been used to design wide-band voltage controlled oscillators (VCOs) [6-9], which are the core used to design an ILFD. However, the design of divide-by 3 ILFD with active inductor has not been studied in literature. This article presents a divide-by-3 ILFD with active inductors to lower the chip area. The proposed divide-by-3 ILFD has a wide locking range. In conjunction with a master VCO, the ILFD can be used as a frequency conversion scheme in a transceiver.

2. CIRCUIT DESIGN

The operating principle of a tunable active inductor (TAI) divide-by-3 ILFD is shown in Figure 1(a). This figure shows the basic small-signal circuit for a TAI oscillator, where the LC-tank is composed of a TAI and a capacitor. The oscillation frequency is determined by the inductance of TAI and the capacitance of capacitor. The negative conductance is used to compensate for the tank loss, not shown in Figure 1(a) for simplicity. The TAI divide-by-3 ILFD shown in Figure 1(b) is basically an oscillator, where transistors (M1–M6) are used to emulate a differential TAI, which in conjunction with a pair of varactors forms the resonator. The cross-coupled transistors M7 and M8 are used to generate negative conductance to compensate for the loss from the LC-tank. The inductance of TAI and capacitance of varactor plus the parasitic capacitors in parallel with the varactors determine the oscillation frequency. Two-injection MOSFETs M9 and M10 with the drain connected to the two ports of the differential TAI are used to couple an external differential injection signal to the resonator. The bias V_{inj} of M9 and M10 also can be used to control the operation frequency because it affects the dc bias of TAI transistors and the small signal of TAI varies with dc bias point. An external balun T1 is used to convert a single-ended input from a signal source to a differential signal. Two passive inductors are shown and they can

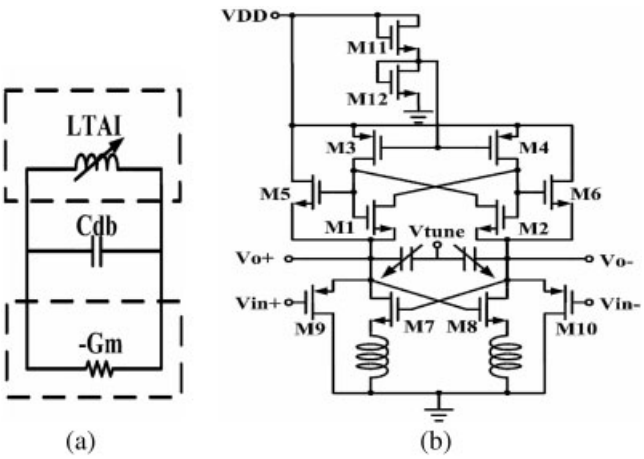

Figure 1 (a) Equivalent circuit of TAI oscillator. (b) Schematic of the proposed TAI divide-by-3 ILFD